JGR Earth Surface

RESEARCH ARTICLE
10.1029/2020JF005918

Rapidly Migrating Secondary Bedforms Can Persist on the Lee of Slowly Migrating Primary River Dunes

J. Y. Zomer[1], S. Naqshband[1], B. Vermeulen[1], and A. J. F. Hoitink[1]

[1]Department of Environmental Sciences, Hydrology and Quantitative Water Management Group, Wageningen University & Research, Wageningen, Netherlands

Key Points:

- High-resolution bed elevation scans demonstrate the migration of trains of superimposed bedforms over active primary dunes
- Superimposed bedforms can persist when travelling over the lee sides of low-angle primary dunes
- Sediment transport rates associated with secondary bedform migration exceed estimates based on conventional methods of primary dune tracking

Correspondence to:
J. Y. Zomer,
Judith.Zomer@wur.nl

Citation:
Zomer, J. Y., Naqshband, S., Vermeulen, B., & Hoitink, A. J. F. (2021). Rapidly migrating secondary bedforms can persist on the lee of slowly migrating primary river dunes. *Journal of Geophysical Research: Earth Surface*, *126*, e2020JF005918. https://doi.org/10.1029/2020JF005918

Received 24 SEP 2020
Accepted 21 JAN 2021

Abstract Trains of secondary bedforms, superimposed on primary dunes, have been observed in rivers worldwide. To date, it has remained unclear how these secondary bedforms affect the sediment transport dynamics in a fluvial system. In this study, a field campaign was conducted to acquire a data set with a high spatial and temporal resolution, enabling to track secondary bedform migration. Results show that two distinct scales of bedforms are actively migrating. In parts of the study area, superimposed bedforms fully dissipate at the lee slope of the underlying primary dune, suggesting that the secondary bedforms contribute to the migration of the primary dune. In other parts, however, superimposed bedforms persist on the lee slope and in the trough of the primary dune. The steepness of the primary lee slope seems to control this. We calculated the sediment transport rates associated with both primary and secondary bedform migration, based on dune tracking. The sediment transport associated with secondary bedform migration is of the same order of magnitude, and even exceeds the transport associated with primary dune migration. This implies that secondary bedforms play a crucial role in the transport of bedload sediment, and cannot be ignored in the quantification of sediment transport based on dune tracking.

1. Introduction

Subaqueous dunes are the building blocks of sand-bedded rivers, affecting flood risk, navigation and the stability of infrastructure (Julien et al., 2002; Kostaschuk, 2000; Wilbers, 2004). Dune migration also plays a key role in the transport of bed sediments (Ashley, 1990; Engel & Lau, 1980; Nelson et al., 1993, 1995; Simons et al., 1965). Especially under conditions where most of the sediment is transported as bedload, in close contact with the riverbed, transport rates are closely related to the migration of bedforms. Bed shear stress, imparted by the flow, increases on the stoss side, transporting sediment downstream and eroding the dune stoss. On the lee sides of the dunes, bed shear stress decreases and particles are deposited (Ashley, 1990; Simons et al., 1965). Where bedload transport is responsible for a major portion of the transported sediment, estimations of the sediment flux can be made based on dune migration rates inferred from repeated bed elevations scans (McElroy & Mohrig, 2009; Simons et al., 1965). This approach is complicated in regions where multiple scales of dunes and other bedforms are observed. It is unclear how these different scales interact and contribute to sediment dynamics.

In river systems worldwide, smaller secondary bedforms have been observed, superimposed on larger primary dunes (Carling et al., 2000; Cisneros et al., 2020; Galeazzi et al., 2018; Harbor, 1998; Parsons et al., 2005; Wilbers & Ten Brinke, 2003). The terms superimposed bedform and superimposed dune sometimes refer to the superimposition of a slightly smaller bedform upstream of the crest of the primary bedform, studied in relation to the ripple-dune transition and dune splitting (Warmink et al., 2014). Here, we use these terms exclusively to refer to the superimposition of trains of secondary bedforms that are significantly smaller than the underlying primary dunes.

Different processes have been described that promote superimposition of smaller-scale bedforms (Ashley, 1990; Martin & Jerolmack, 2013; Reesink et al., 2018). After a peak in discharge, larger dunes, created during high flow, become inactive and superimposed dunes emerge, adopting a scale that is in equilibrium with the new flow conditions (Martin & Jerolmack, 2013). The superimposed dunes then cover both the stoss and lee sides of the primary dunes (Allen, 1966; Allen & Collinson, 1974; Davies, 1982) and are responsible for all the bedload transport (Wilbers, 2004). However, superimposed bedforms have also been

observed under steady flow conditions. To explain these observations, it has been argued that the primary dunes generate a boundary layer in which superimposed bedforms can develop and are stable (Ashley, 1990; Rubin & McCulloch, 1980; Smith & McLean, 1977).

Venditti et al. (2005b) studied the dynamics of multiple scales of migrating bedforms under steady flow conditions through laboratory experiments and confirmed the superimposition of multiscale bedforms under steady flow conditions. They found that the small superimposed bedforms form downstream of the upstream, primary lee side and dissipate at the lee side of the next primary dune. Furthermore, they found that the superimposed bedforms migrate significantly faster than the larger dunes and that the associated sediment transport is comparable to the transport rates measured based on primary dunes. They concluded that sediment transport rates seem invariant to the observed scale of bedforms and that the migration of superimposed bedforms is the agency by which the primary dune migrates. In their study, the superimposed bedforms travel over the stoss side and collapse at the lee side.

It is unknown, however, if the same conclusion can be drawn for multiscale dune migration in field conditions. Dunes in flumes, formed in limited water depth and high Froude number flows, are typically asymmetrical and have steep lee side angles. In natural rivers, so-called low-angle river dunes are often formed (Bradley & Venditti, 2017; Naqshband & Hoitink, 2020; Naqshband et al., 2014a; Van der Mark et al., 2008). Lee side angles observed in natural rivers can be even smaller than 10° (Cisneros et al., 2020; Hendershot et al., 2016; Lefebvre et al., 2016; Ten Brinke et al., 1999). In contrast to high-angle dunes, flow separation for low-angle dunes is not or only intermittently present (Bradley et al., 2013; Holmes & Garcia, 2008; Kostaschuk & Villard, 1996; Kostaschuk et al., 2009; Kwoll et al., 2016). It is unclear if the bedform behavior observed by Venditti et al. (2005b) in flume experiments would occur under conditions in which low-angle dunes develop. Galeazzi et al. (2018) described a river section in which superimposed bedforms were in some cases limited to the stoss of the low-angle primary dunes, whereas in other cases they persisted over the lee slope. Galeazzi et al. (2018) did not study the dynamics of these bedforms. It is unknown if superimposed bedforms contribute to the migration of the primary dune or form an additional transport mechanism where they persist over the dune lee side.

The dynamics of superimposed bedforms in sand-bedded rivers have not often been studied in field conditions. One important reason for this is that usually the temporal resolution of repeated bed elevation measurements is not high enough to resolve the migration of small bedforms (Claude et al., 2012; Kleinhans et al., 2007). In addition, a high spatial resolution is required to enable proper estimates of the morphological properties of superimposed bedforms. For the purpose of investigating the dynamics of small-scale superimposed bedforms, we acquired a data set with an extraordinarily high spatial and temporal resolution. The aim of this study is to investigate multiscale bedform migration in a fluvial system and to determine the importance of secondary bedform migration in the quantification of sediment transport rates.

2. Methodology

2.1. Field Campaign

A field campaign was conducted on October 11, 2018 in the river Waal, the main distributary branch of the Dutch river Rhine (Figure 1). A bathymetric survey was conducted over a reach of approximately 500 m. Within this area, depths range between −1 and −4 m + NAP. The water level during the campaign was 2.2 m + NAP at the city of Tiel, approximately 5 km upstream and 1.1 m + NAP at Sint Andries, approximately 7 km downstream. Herein, NAP refers to Normaal Amsterdams Peil, which is the Amsterdam Ordnance Datum. During the campaign, large primary dunes were present with lengths predominantly between 50 and 180 m and heights up to 1.6 m, and superimposed secondary bedforms with lengths and heights mostly below 5.5 and 0.35 m, respectively.

Bed elevations were measured using a boat-mounted multibeam echosounder (MBES). In addition to the bathymetric survey, the field campaign included eight repeated measurements of a cross-sectional area. The time interval between each of the eight measurements was approximately 15 min. Each repeated measurement consisted of five parallel boat tracks, such that the bed areas covered by the multibeam were partly overlapping. Together, these tracks covered an area of about 220 × 50 m. During a measurement cycle, the

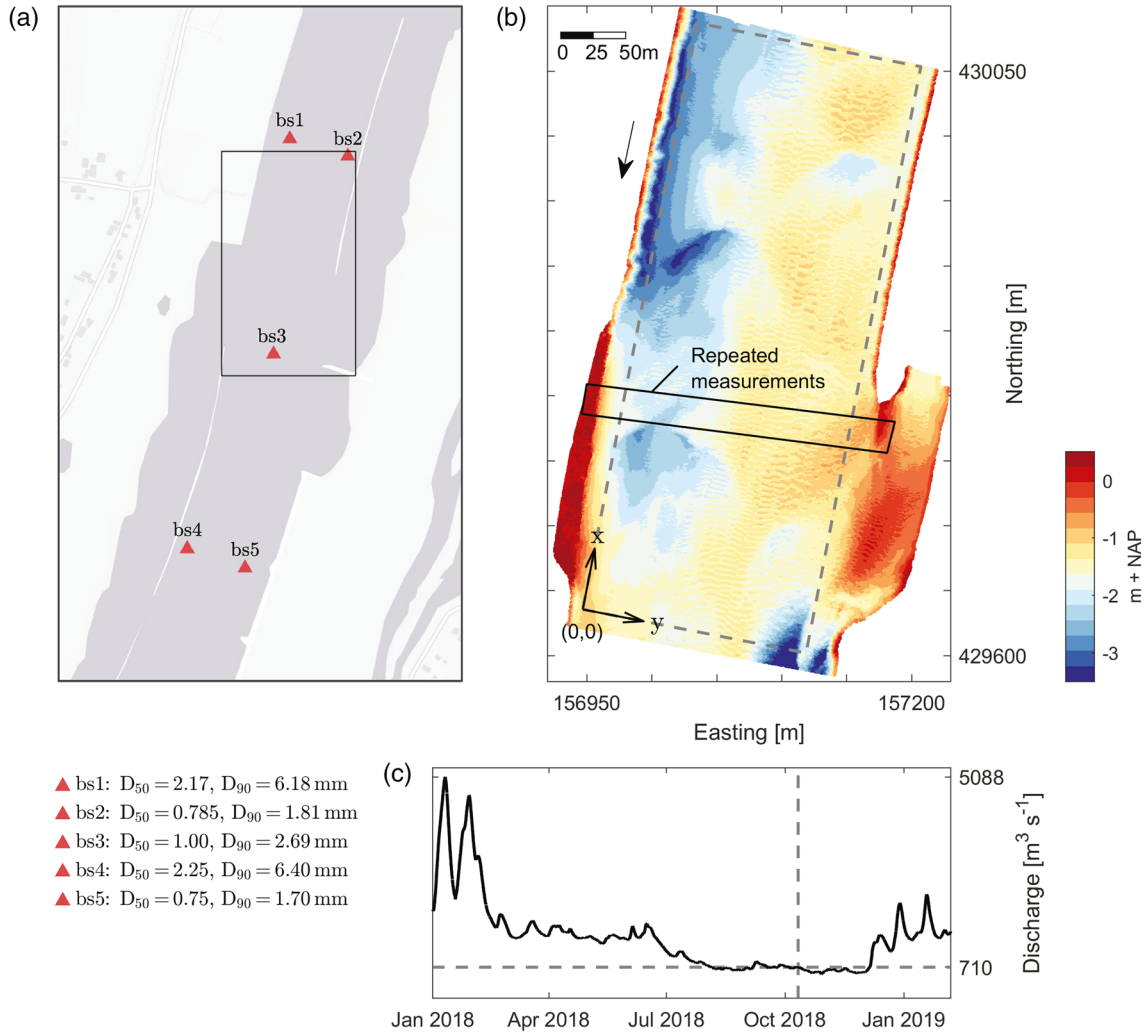

Figure 1. Field study area. (a) The location of the study area, in the Waal river near Ophemert. The locations where bed samples were taken are indicated; (b) the bathymetry as surveyed on October 11, 2018. The arrow indicates the flow direction, which is from the northeast to the southwest. The earth coordinates (Easting, Northing) are in the EPSG:28992 system; (c) the discharge at Tiel, approximately 5 km upstream of the study area. On October 11, $Q = 710\ m^3s^{-1}$.

boat started in one corner of the survey area. It navigated the five tracks and then went back to the initial position, to start the next cycle. In addition to an MBES, an acoustic Doppler current profiler (ADCP) was mounted on the boat to measure flow velocities.

The data of the dedicated field campaign were complemented by MBES data made available by the Dutch Ministry of Infrastructure and Environment, Rijkswaterstaat (RWS). These data are part of a larger data set, which was acquired to monitor the river bed to ensure that the water depth is sufficient for ships to pass through. The RWS data were acquired with an interval of six days, on October 9 and October 15. At the location of the field site, information on the bed grain size distribution is also available, based on samples that have been taken on November 24, 2017 using a Hamon grab (de Ruijsscher et al., 2020b; Eleftheriou & Moore, 2013). The 50th (D_{50}) and 90th percentile sediment diameter (D_{90}) were determined following the approach of de Ruijsscher et al. (2020a) and are shown in Figure 1 (*bs*1 through *bs*5).

2.2. Data Processing

The MBES data were processed as point clouds with a spatial resolution of $1 \times 1 \times 1$ cm. The coordinates were transformed to a Cartesian coordinate system that aligns with the central axis of the river, and has its origin in the lower left corner of the bathymetric map, as indicated in Figure 1. The point clouds were subsequently interpolated on an equidistant grid with a cell size of 0.1 m through inverse distance weighted interpolation. The interpolation was done with the Geospatial Data Abstraction Library (GDAL) (GDAL/OGR contributors, 2020). For the bathymetric map, the outline of the grid is indicated in Figure 1.

The coordinates of the repeated transects were transformed to the same Cartesian coordinate system as the bathymetric map and interpolated on the same 0.1 m equidistant grid. In addition to the spatial interpolation, the repeated transects were linearly interpolated in time. After the spatial interpolation, at each grid cell, eight elevation (z) values were available, with their corresponding time stamps. Through linear interpolation, the elevation values at a grid node were interpolated to eight predefined timestamps with a fixed time interval of 14.4 min. The temporal interpolation was done, because the time intervals between point measurements within a measured transect were relatively large compared to the time intervals between repeated transects.

The MBES data made available by RWS were processed as 1×1 m grids. The coordinates of the grid nodes were transformed and the values were interpolated on a 1×1 m grid with the same origin and orientation as that of the bathymetric map.

Further processing of all gridded data is performed for each individual transect, where each transect is aligned with the central axis of the river, and corresponds to one $y-$coordinate of the grid.

The ADCP data were processed using the Matlab toolbox ADCPTools (Vermeulen et al., 2014). The ADCP data were acquired with a bin size of 0.25 m and a blanking distance at the transducer of 0.25 m. Velocity values in the lowest 6% of the measured water column were excluded from further analysis. The remaining flow velocities were fitted on a mesh with a horizontal resolution of 5 m and a vertical resolution of approximately 0.25 m. The obtained velocity values were interpolated toward the surface through nearest neighbor interpolation and toward the bed through linear interpolation, assuming zero-velocity at the bed. The extrapolated values were included in computations of the depth-mean velocity.

A value for the shear velocity was calculated for each velocity profile following the approach of Hoitink et al. (2009), assuming the velocity profiles can be described by the law of the wall up to the surface:

$$u(\sigma) = \frac{u_*}{\kappa}(\ln\sigma + 1) + U, \tag{1}$$

where u_* is the shear velocity, κ is the Von Karman constant, σ is the relative depth, and U is depth-mean velocity. Fitted parameters with an adjusted $R^2 < 0.9$ were excluded from further analysis. The shear velocity was used to compute the bed shear stress: $\tau_b = u_*^2\rho$.

2.3. Separation of Bedform Scales

The superimposed bedforms were separated from the underlying morphology, including primary dunes, to study the superimposed bedforms and primary dunes separately. The raw data were filtered based on a LOESS (locally estimated scatterplot smoothing) algorithm (Cleveland, 1979; Greenslade et al., 1997; Schlax & Chelton, 1992). Because the high-frequency fluctuations in the signal associated with secondary bedforms have a relatively large amplitude, sufficient data points have to be included in the scatter plot prior to smoothing. In sections where the underlying morphology does not change much over short spatial scales, LOESS performed well. However, at locations where the change in elevation is significant, especially at primary lee sides, the filtering method does not perform well, as the LOESS curve does not match the primary morphology.

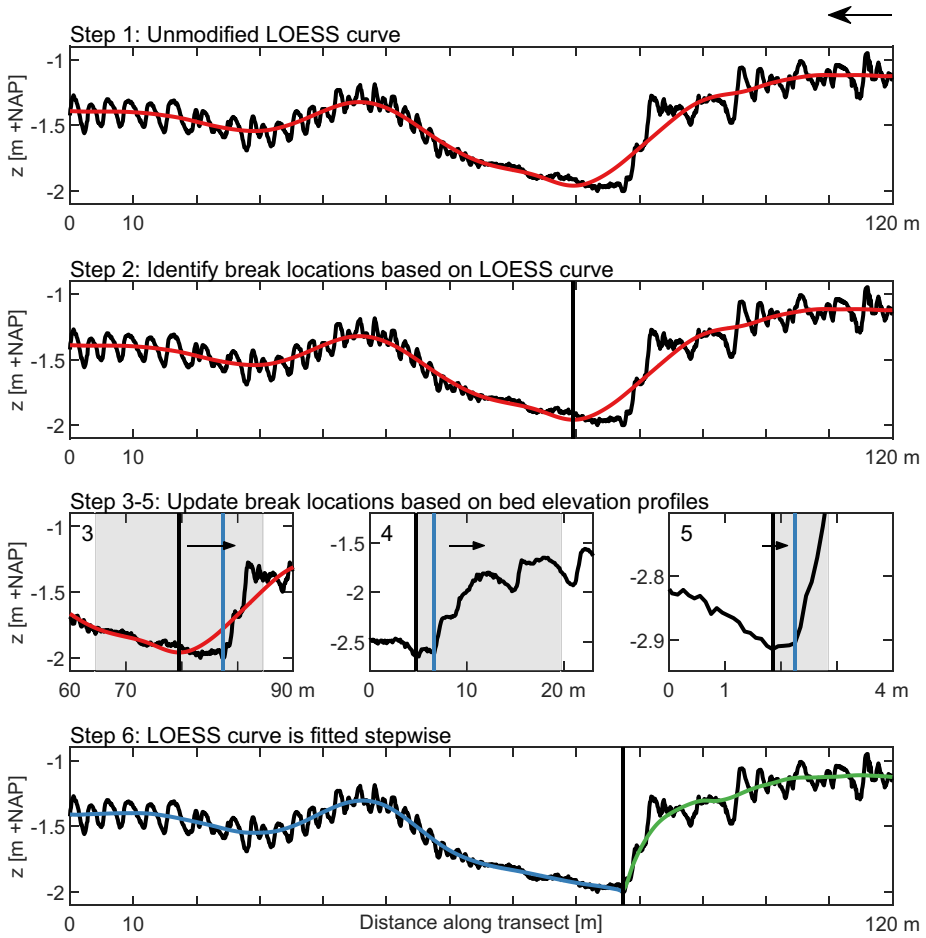

Figure 2. A schematic overview of the method applied to separate the superimposed bedforms from the underlying morphology. Step 1: The unmodified LOESS curve does not match the primary morphology at the primary lee side and trough; Step 2: Detection of the break location based on the LOESS curve, which is to be adjusted. Steps 3–5: The break location is updated toward the slope discontinuity in the bed elevation signal, the transition from trough to the primary lee. This location is treated as a break in the filtering. Step 6: The algorithm is used for incremental LOESS filtering between the break locations. Steps 1–3 and 6 show the same bed elevation profile. For Steps 4 and 5, different elevation profiles are shown. LOESS, locally estimated scatterplot smoothing.

The unintended smearing of the primary dune morphology was addressed by introducing breaks at the locations where the unmodified LOESS curve significantly departs from the dune trough and from the slope of the dune lee. An illustration of the applied method is provided in Figure 2. In the first panel (Figure 2: Step 1), an example of a bed elevation signal (black) is shown, along with the unmodified LOESS curve (red). In the second step, the locations are identified where a break should be applied, based on this LOESS curve. These breaks were identified based on two criteria. The first criterion is that the break should be in the center of a primary dune trough. The centers of the primary dune troughs were initially approximated as local minima of the unmodified LOESS curve. The second criterion is that the maximum slope of the LOESS curve between the trough and the nearest, upstream crest, the next local maximum of the LOESS curve, should be higher than a specified value, here set at 1.72°. An example is shown in Figure 2: Step 2.

Subsequently, in the third to the fifth step the exact location where the breaks in the trough centers are set is updated (Figure 2: Steps 3–5). The breaks should be located at the transition from the trough to the lee. In the third step, the minimum z − value of the original signal near the break is located (within 15 m up or downstream of the break). In the fourth step, all local minima are identified within a window between the breakpoint found in the previous step and 15 m upstream. If there are local minima that have a maximum vertical distance of 0.05 m with the absolute minimum, the most upstream of these local minima is selected

as the new break location. This step is especially relevant if secondary bedforms are present in the trough. In the fifth step, the $z-$ values from the breakpoint to 1 m upstream are considered. If the next value is less than 5 mm higher (corresponding to a slope of 2.9°) the breakpoint is updated to that location.

In the sixth and final step, the LOESS curve is fitted stepwise, starting at the most downstream section, up to the first break. This implies that the LOESS curve is fitted through the stoss downstream of the break. For the next section, the LOESS curve is forced to connect to the previous LOESS curve that ends at the breakpoint. This is achieved by adding artificial data points at the break. In this way a LOESS curve for each section of a transect is fitted.

2.4. Bedform Properties

The properties of secondary bedforms are based on the filtered data and were determined following the method of Van der Mark and Blom (2007). In this method, troughs and crests are identified as minima and maxima between zero crossings. The bedform length is defined as the distance between two troughs. The bedform height was calculated both from trough to the next bedform crest and from crest to the next bedform trough. The height of a bedform was subsequently defined as the average of these two. To compute the lee side slope, 1/6th part of the slope was removed both at the crest and at the trough edge of of the slope. The slope angle was then approximated by a linear fit though the remaining central part (Van der Mark & Blom, 2007).

Random irregularities also cross the nulline and are as a result wrongly identified as bedforms. All identified bedforms of which the height was smaller than four times the standard deviation of local elevation values (a total of 15 values) were excluded from the results.

Primary dune length and height were also determined following Van der Mark and Blom (2007). The primary dune height was calculated from the trough to the upstream crest. The lee side slope was determined as the maximum bed elevation slope between the trough and the upstream crest. This approach was followed because, first, the primary dune morphology was filtered and did not include irregularities that can affect the observed maximum lee side slope. A second reason is that flattened crests of primary dunes in the study area would lead to large discrepancies between locally observed lee side slopes and the lee side slopes determined following the approach of Van der Mark and Blom (2007). Toward the left and right outer edges of the primary dunes, where the dune transitions to a flat bed, dune detection results in small heights and lee side angles. To exclude these values, datapoints with heights smaller than 10% of the maximum dune height were filtered out.

2.5. Sediment Transport Associated With Bedform Migration

The sediment transport rates associated with both primary and secondary bedform migration were calculated based on dune tracking. Various methods based on dune tracking have been developed, commonly based on the one dimensional Exner equation for mass conservation of sediment, valid for steady flow:

$$(1-p)\frac{\delta\eta}{\delta t}+\frac{\delta q}{\delta x}=0, \tag{2}$$

where p is the porosity of the bed (−), η is the local bedform elevation with respect to the base level of the bedform, $\eta = z - z_0$, (m), and q is sediment transport per unit width (m^2s^{-1}).

Based on the one-dimensional Exner equation (Equation 2), the following equation for the sediment transport associated with bedform migration can be derived (McElroy & Mohrig, 2009):

$$q=(1-p)V_c\eta+q_0, \tag{3}$$

where V_c is the dune migration rate (ms^{-1}) and q_0 a constant of integration. The derivation of Equation 3 has been described by McElroy and Mohrig (2009) and is based on the assumption that migrating bedforms

are unchanging under steady flow conditions. Further assuming that the bedload transport is zero in the trough ($q = 0$ at $\eta = 0$), $q_0 = 0$, leads to:

$$q = (1 - p)V_c\eta \tag{4}$$

Often, q is integrated over the bedform, introducing the dune height and a shape factor β, replacing η. Here, we did not compute the transport rate per bedform, but computed an average q_s per transect.

V_c, the bedform migration rate, is computed for each transect through the cross-correlation of two bed elevation scans. The migration rate is then the distance traveled divided by Δt. The local bedform elevation, η, is the bed elevation with respect the bedform base level z_0. The bedform base level was computed through linear interpolation between bedform troughs. The porosity, p, is assumed to be 0.36 (Allen, 1985).

The eight repeated measurements of the cross-sectional area (Figure 1) were used for the computation of the sediment transport rate associated with secondary bedform migration. For transects with $y \leq 70$ m, the migration rates,V_c, were computed based on bed elevation scans with time intervals of $\Delta t = [14.4, 28.8, 43.2]$ minutes. Considering these time intervals and the total number of bed elevation scans available, 18 different combinations of two bed elevation scans were available, resulting in 18 separate estimations of the migration rate, V_c. For transects with $y > 70$ m, the migration rates were computed with larger time intervals, $\Delta t = [72.0, 86.4, 100.8]$. These time intervals enable a total of six different combinations of bed elevation scans. The difference in time intervals used for the two sections corresponds to a difference in migration celerity.

The local bedform elevation, η, was computed per transect between the first and last trough (so only for bedforms fully included in the measured area). The bed elevations were computed for each of the eight repeated measurements. The averaged values were used to compute the sediment transport.

The sediment transport rate associated with primary dune migration was computed based on the MBES data acquired on 9 and 15 October. Here, a moving-average dune migration rate was computed.

The sediment transport rates found based on dune tracking were compared to transport rates calculated with a transport formula. Here, we used the equation of Engelund and Hansen (1967). This equation was selected because it is applicable to a sandy, dune-covered bed. Following this approach, the nondimensional sediment discharge Φ is computed as:

$$\Phi = 0.1\theta^{5/2} / \mathrm{f}, \tag{5}$$

where θ is the Shields stress computed from the bed shear stress values based on the ADCP measurements and f is the friction factor. The bed sediment discharge per unit width [m^2s^{-1}] then reads:

$$q_s = \Phi\sqrt{(s-1)gD_{50}^3}, \tag{6}$$

with g is the acceleration of gravity [ms^{-2}], s is the relative density of sediment grains (ρ_s/ρ_w) and D_{50} is the median grain size [m]. The values of D_{50} across the channel were computed based on the bed samples presented in Figure 1. The y-coordinates of the samples were transformed into the Cartesian coordinate system of the grids. The samples taken in the western and eastern river sections were averaged to get one value in the western section and one value in the eastern section. Together with the central sample, *bs*3, values for D_{50} were obtained over the full river width, i.e. as a function of the y-coordinate, by linearly interpolating in between sample locations and extrapolating toward the river banks using nearest neighbor extrapolation.

The transport equation of Engelund and Hansen (1967) computes the total transport of bed sediments, including the suspended sediment transport. To enable good comparison with the estimates based on dune tracking, which only relate to the bedload mode, we assessed whether bedload transport was the dominant sediment transport mode. A common parameter to assess the relative importance of bedload transport to suspended load transport is the ratio of the bed shear velocity and the particle fall velocity, u_*/w_s, also referred to as the suspension number (Bagnold, 1966). Bedload transport is the dominant transport

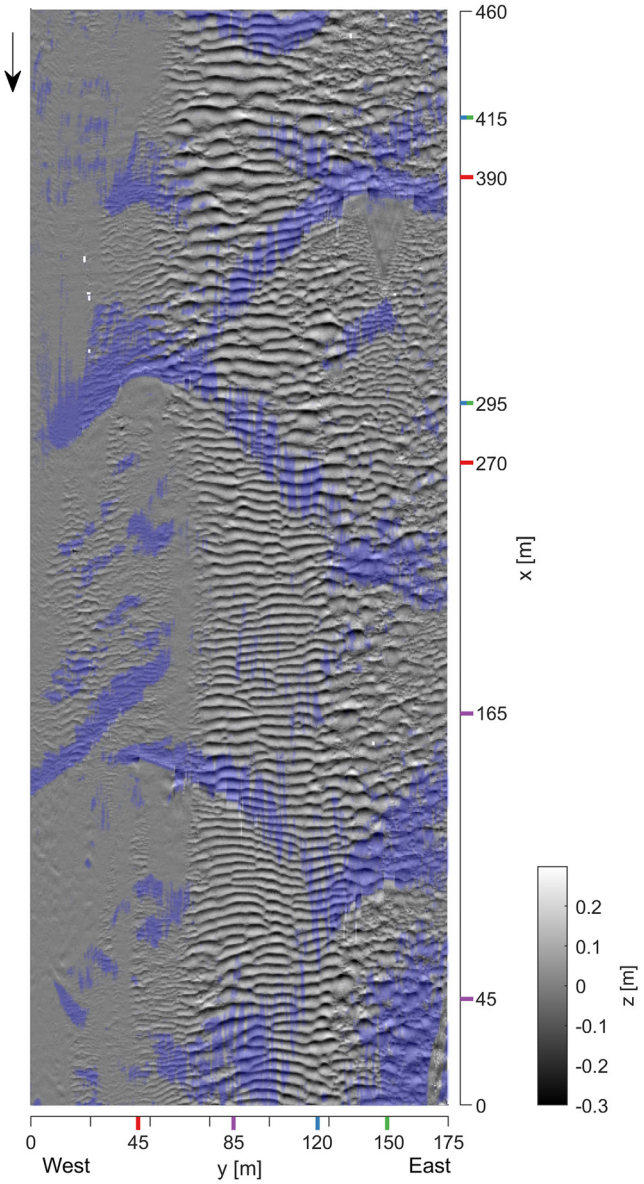

Figure 3. Morphology of superimposed bedforms, extracted from the bathymetric map. The purple areas indicate leeside slopes of primary dunes. The arrow indicates the flow direction, which is roughly from north to south.

mode for $u_*/w_s < 1$. According to Van Rijn (1984), initiation of suspension starts at $u_*/w_s = 0.4$. The particle fall velocity was calculated following Cheng (2009):

$$w_s = \sqrt{\frac{4}{3}(s-1)\frac{gD_{50}}{C_D}}, \tag{7}$$

with the drag coefficient C_D defined as:

$$C_D = \frac{432}{D_*^3}(1 + 0.022D_*^3)^{0.54} + 0.47(1 - \exp(-0.15D_*^{0.45})), \tag{8}$$

where D_* is the dimensionless grain diameter.

3. Results

3.1. Morphology of Superimposed Bedforms

The morphology of the superimposed bedforms, which has been separated from the underlying bathymetry, is shown in Figure 3. The secondary bedforms are superimposed on lunate primary dunes. The purple areas indicate where primary lee slopes are positioned. The lee sides of the primary dunes are defined as slopes with an aspect angle between 112.0° (southeast) and 247.5° (southwest). The western section is deeper than the eastern section, as visualized in Figure 1. Figure 3 indicates a high lateral variability of the superimposed bedforms. In the western part of the river section, roughly between $y = 0$–70 m, superimposed bedforms are very small and some regions are poorly resolved by the MBES measurements. The middle section of the riverbed ($y = 70$–130 m) is covered with larger, two-dimensional bedforms. Here, the superimposed bedforms are clearly visible also on the lee slopes of primary dunes. In the eastern river section ($y = 130$–175 m), superimposed bedforms are also clearly visible, but here they are much more irregular in shape and size. At $x = 365$ m, a triangular section is visible, directly downstream of a primary lee slope, where superimposed bedforms have dissipated.

In Figure 4, four bed elevation profiles are shown. The first plot shows a profile at $y = 45$ m. Very small secondary bedforms are superimposed on an asymmetrical dune with a steep lee side slope. Directly downstream of the lee side slope, superimposed bedforms are absent. The second and third plot show profiles from the central river section, where secondary bedforms are larger. These profiles show small primary lee side angles over which the secondary bedforms persist. In the third profile, at $y = 120$ m, the superimposed bedforms are significantly smaller downstream of the primary lee side. They grow again in the downstream direction. The fourth plot shows a profile at $y = 150$ m. Downstream of primary lee side slopes, superimposed bedforms entirely disappear and start to develop roughly 25 m further downstream.

Figures 5a–5c show the properties of the secondary bedforms and their position with respect to the y-axis. The results presented in Figures 5a–5c are based on a selection of transects, all with a lateral interval of 10 m (every 100th transect). Figures 5a–5c show that bedforms in the western section ($y \leq 70$ m) are smaller compared to bedforms in the central and eastern sections. Bedforms in the central section (70 m $< y \leq 135$ m) on the other hand are larger, have a high aspect ratio and lee side slope. Figures 5d–5f show the distributions of bedform properties per section as well as the cumulative histogram. The median bedform length per section is 2.3 m (West), 4.3 m (center), and 3.5 m (East). The median height per section is 0.10 m (West),

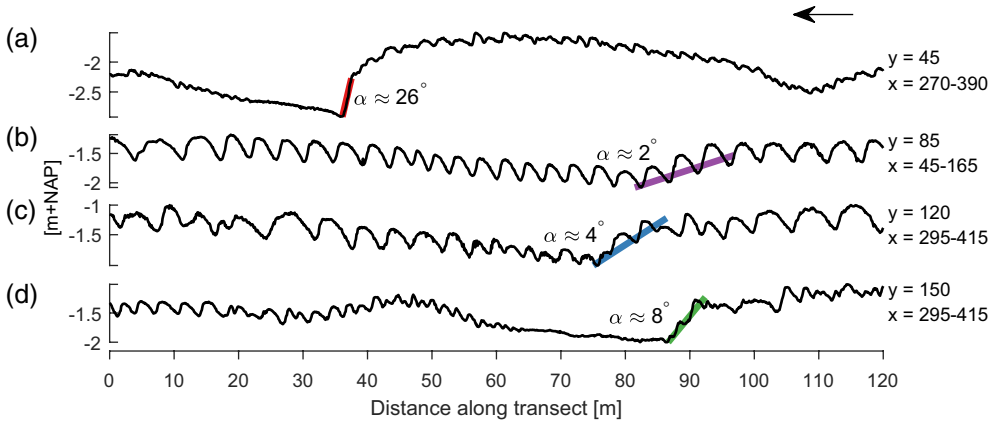

Figure 4. Bed elevation profiles of selected transects with estimated primary lee side slopes, showing morphodynamic evolution of superimposed bedforms.

0.30 m (center), and 0.21 m (East). The median lee side slope per section is 11.8° (West), 20.0° (center), and 15.5° (East).

Figures 5g–5j show the primary dune properties, indicating that dune lengths do not significantly vary per section, but primary dunes are highest and steepest in the western section, whereas lee side slopes in the central and eastern sections are comparatively low.

3.2. Bedform Migration

Figure 6 shows the digital elevation models (DEMs) of difference of two repeated elevation scans, where $\Delta z = z_{\text{new}} - z_{\text{old}}$. Positive values indicate a net deposition of sediment and negative values indicate a net erosion between two elevation scans. If the time span between two elevation scans is appropriate, the DEM of difference reflects bedform migration, visualizing sediment deposition on the bedform lee and erosion of the stoss.

In Figure 6, the left plot shows the DEM of difference based on MBES data acquired on 9 and 15 October. This plot shows the migration of the larger, primary dunes over a period of 6 days. The two plots on the right show two DEMs of difference based on the measurements repeated within one day. These plots indicate the migration of secondary bedforms over a time period of approximately 28.8 min and 100.8 min. The DEMs of difference indicate that in the same time period, both primary and superimposed, secondary bedforms are actively migrating.

3.3. Sediment Transport Rates Associated With Bedform Migration

Figure 7a shows a cross-sectional overview of the streamwise velocity. The flow velocity is significantly higher across the western river section, which is also reflected in the depth-averaged flow velocity shown in Figure 7b. Figure 7b further shows the bed shear stress calculated based on the velocity measurements and the ratio of the bed shear velocity u_* and the particle fall velocity w_s, which ranges between 0.12 and 0.54, indicating that bedload transport is the dominant transport mode.

Sediment transport rates associated with primary and secondary bedform migration have been calculated based on the bedform migration celerity V_c and the bedform elevation with respect to the bedform base level $\eta = z - z_0$. The celerity V_c of secondary bedforms was computed per transect and presented in Figure 7c. The bedform elevation η was averaged longitudinally within each transect. Both bedform celerity and the average bedform elevation vary laterally, with a sharp transition around $y = 70$ m. The smaller secondary bedforms in the western section of the river migrate much faster than the larger secondary bedforms in the central and eastern sections.

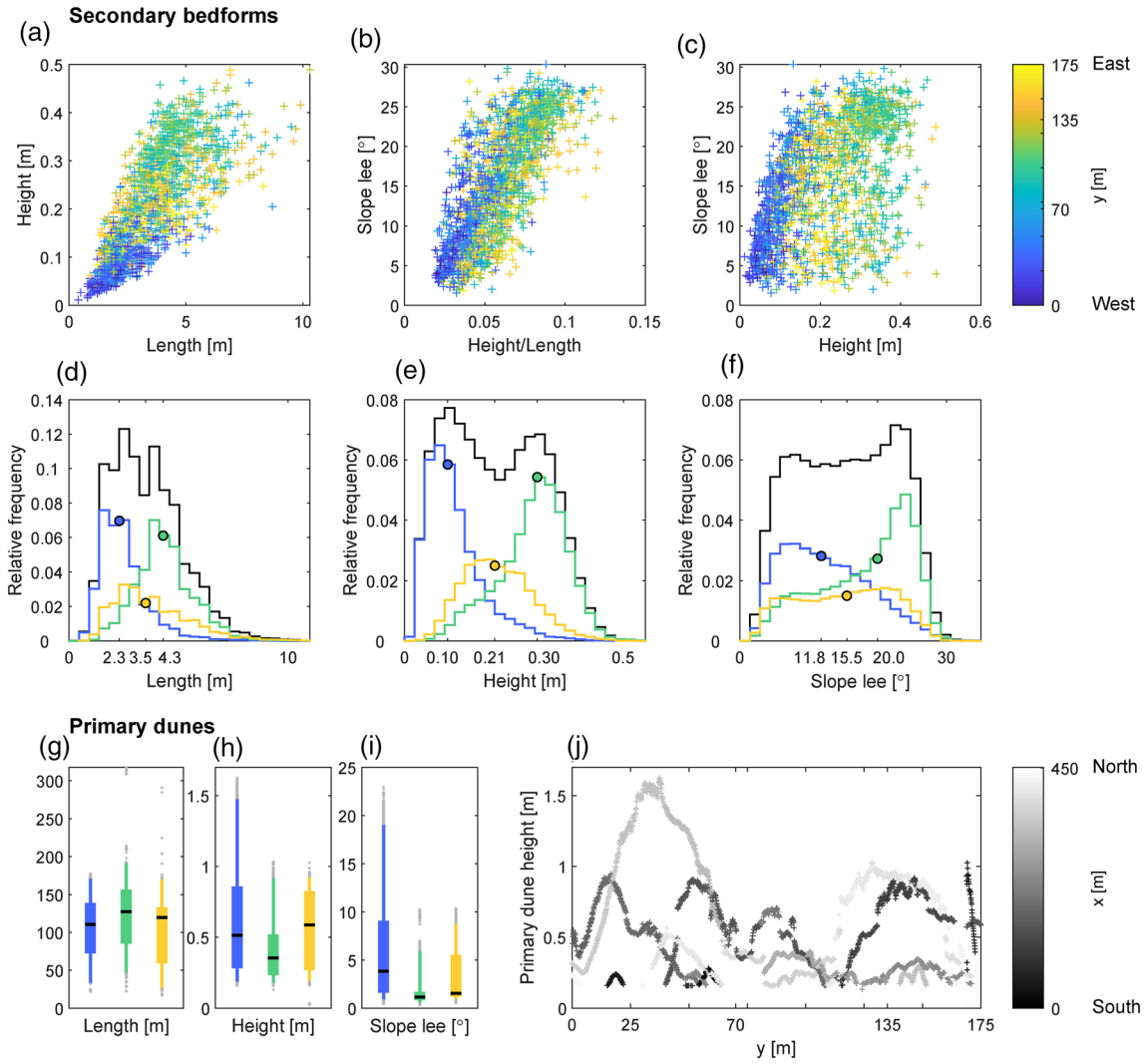

Figure 5. Properties of the secondary and primary bedforms; (a) Secondary length versus height; (b) the aspect ratio (height/length) versus lee slope of seconary bedforms; (c) the secondary height versus lee slope; (d) Histograms of secondary bedform lengths, both per section and the cumulative histrogram; (e) histograms of secondary bedform heights; (f) histogram of secondary lee side slopes; g–i: Boxplots based on the [5, 25, 50, 75, 95]th percentiles of primary dune length, height and lee slopes; (j) Lateral distribution of primary dune height. In plots d–i, blue indicates the western section ($y \leq 70$ m), green indicates the central section (70 m $< y \leq 135$ m) and yellow indicates the eastern section ($y > 135$ m).

Figure 7d shows the bedload sediment transport rates per unit width (q_s) associated with primary and secondary bedform migration based on V_c and η. The propagated uncertainty of the calculated transport rate associated with secondary bedform migration (σ_{q_s}) is calculated according to:

$$\sigma_{q_s} = \mid q_s \mid \sqrt{\left(\frac{\sigma_\eta}{\eta}\right)^2 + \left(\frac{\sigma_{V_c}}{V_c}\right)^2}, \tag{9}$$

assuming the errors of η and V_c are uncorrelated. The quantification of uncertainty includes the variability related to errors in the temporal interpolation of the repeated bed elevation measurements.

There are gaps apparent in the secondary transport calculations; this occurs at locations where bedform celerity is not properly calculated, because either superimposed bedforms are not present, or are not properly resolved. The sediment transport rates associated with primary dune migration were calculated based on the MBES data of October 9 and October 15, 2018.

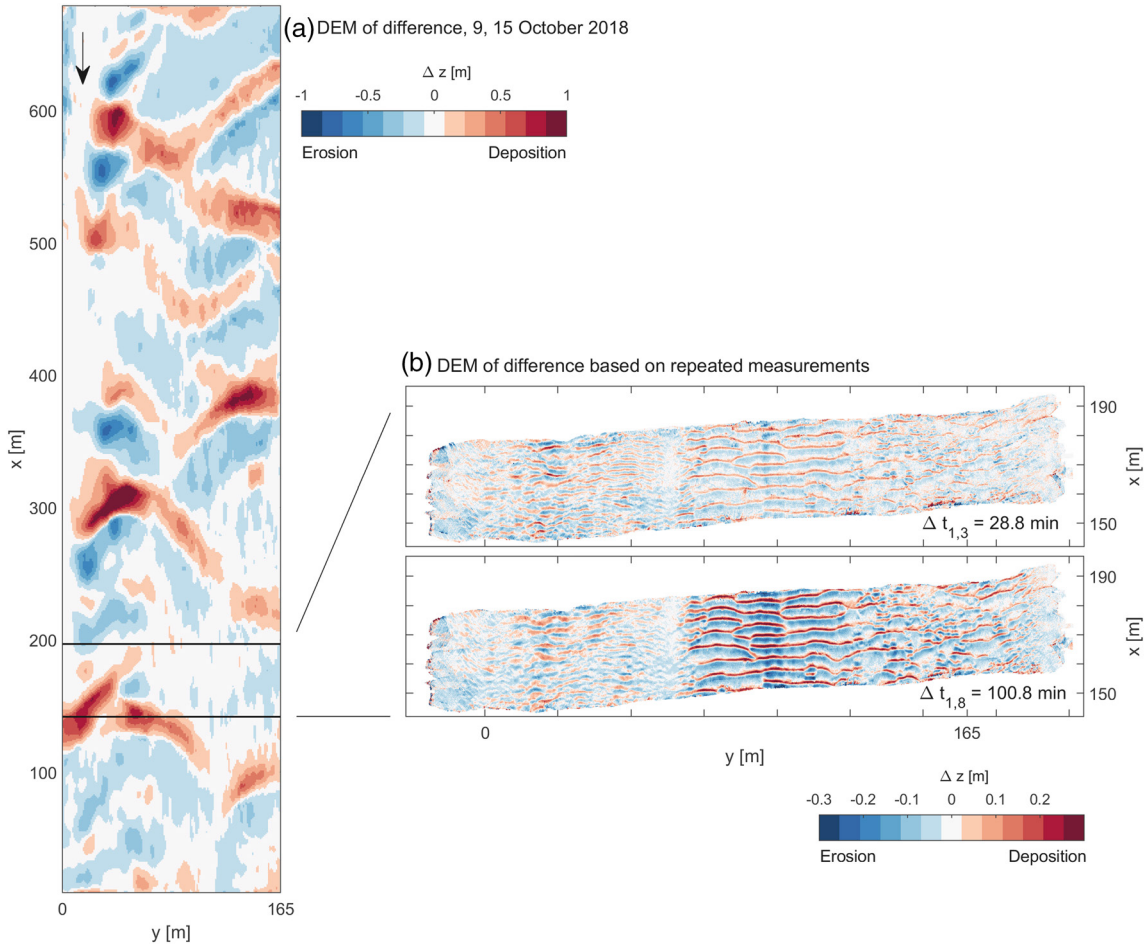

Figure 6. DEMs of difference ($\Delta z = z_{new} - z_{old}$) indicating bedform migration. Red areas represent a net deposition, blue areas net erosion. The left figure is based on MBES data with a time interval of 6 days. The right two figures are based on the repeated measurements during the dedicated field campaign, visualizing the migration of secondary bedforms.

The sediment transport rates, q_s, for primary and secondary bedform migration are of the same order of magnitude. Primary transport is largest around $y = 40$ m and $y = 150$ m and decreases in the central river section. Transport associated with secondary bedform migration significantly exceeds that by primary dunes in the central section of the river. The transport associated with secondary bedform migration peaks around $y = 25$ m and $y = 100$ m, correlating to peaks in dune celerity (at $y = 100$ m) and η (at $y = 25$ m).

Figure 7d further shows the calculated bed sediment transport based on Engelund and Hansen (1967). The calculated transport is of the same order of magnitude as the sediment transport associated with bedform migration. Around $y = 20$ m the transport peaks, which is not reflected in the calculations based on bedform migration. The peak corresponds to a peak in the estimated bed shear stress (Figure 7b).

4. Discussion

Results of bed elevation measurements at different time-scales have been presented. The results indicate that two distinct scales of bedforms are actively migrating within the same river section. The smaller scale bedforms are superimposed on larger, primary dunes and can persist across the lee sides of the primary dunes. The sediment transport associated with the more rapid migration of the smaller superimposed bedforms is of the same order of magnitude as the transport associated with primary dune migration. Averaged over the width of the river, it even shows to be larger.

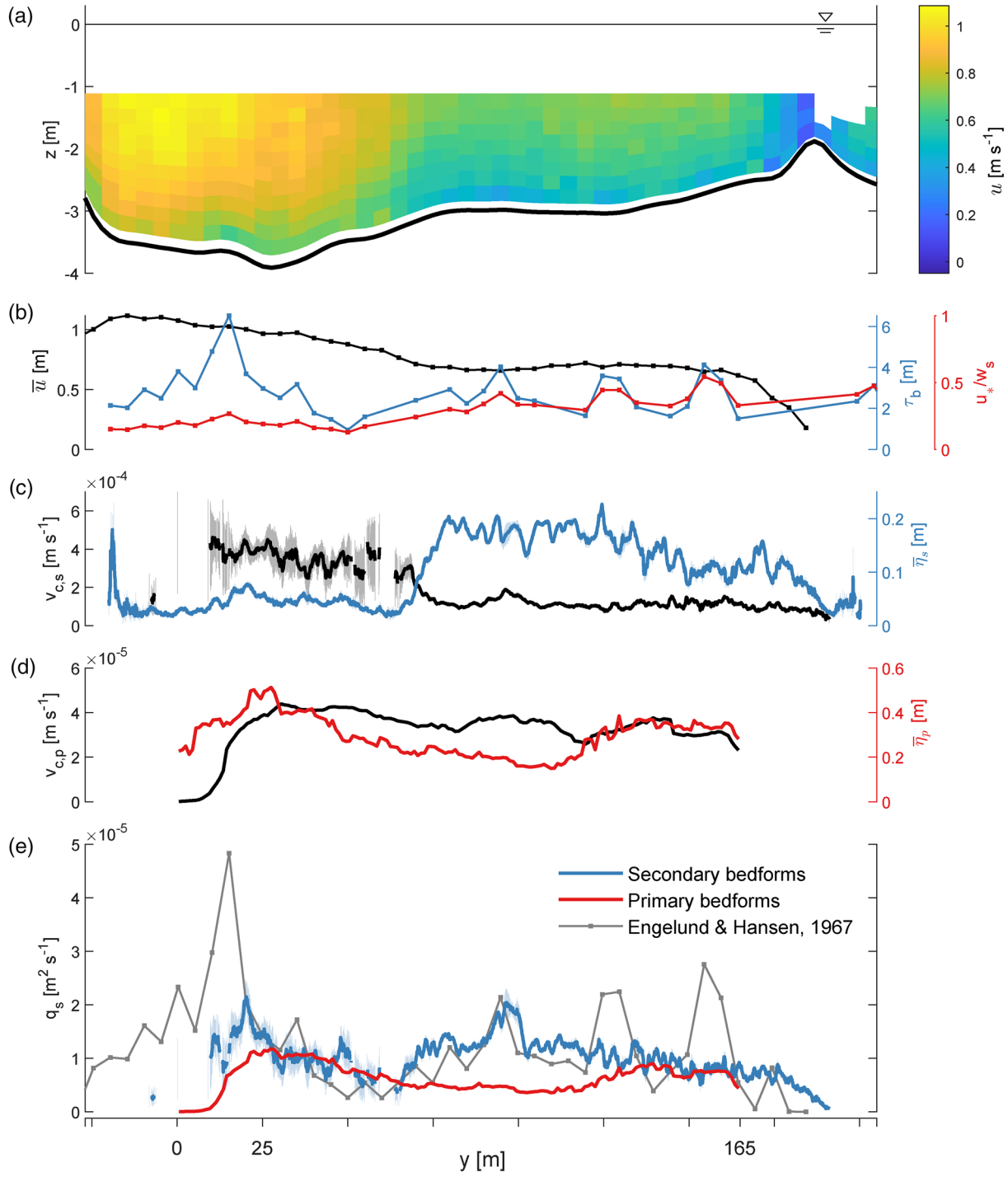

Figure 7. (a) Cross-sectional view of the streamwise flow velocity; (b) The depth-averaged streamwise flow velocity $\overline{u}$, bed shear stress τ_b, and the suspension number u_*/w_s; (c) The migration celerity of secondary bedforms $V_{c,s}$ and the average bedform elevation $\overline{\eta}_s$. The vertical light gray and light blue bars indicate the standard deviation related to $V_{c,s}$ and $\overline{\eta}_s$, respectively; (d) the migration celerity of primary dunes $V_{c,p}$ and the average bedform elevation $\overline{\eta}_s$; (e) sediment transport associated with primary and secondary bedform migration and the bed sediment transport rate calculated following Engelund and Hansen (1967). The vertical light blue lines indicate the propagated uncertainty related to the sediment transport based on tracking of secondary bedforms.

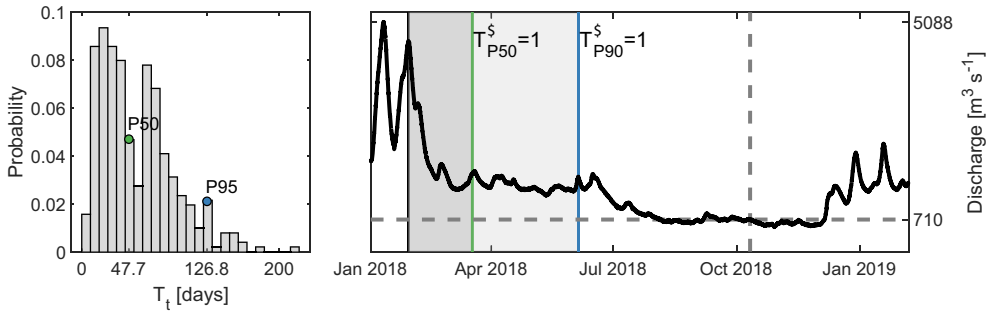

Figure 8. The bedform turnover timescales, T_t (left), computed per dune, per transect, with a median value of 47.7 days and the 95th percentile of 126.8 days. The duration necessary for dunes to adapt to the prevailing flow conditions ($T^* = 1$) is indicated on the right based on both the 50th and 95th percentile of T_t.

4.1. The Superimposition of Secondary Bedforms on the Stoss and Lee of Primary River Dunes

Previous research offers two distinct explanations for the development of trains of superimposed bedforms on primary river dunes. A first explanation for the superimposition of small dunes or ripples on primary sand-bedded dune lee sides is that the superimposed bedforms are the only active bedform scale, whereas the primary dunes have become inactive and are a relict of prior, high discharge conditions (Allen & Collinson, 1974; Martin & Jerolmack, 2013; Myrow et al., 2018). In this case, the superimposed bedforms erode the primary crests and fill up the dune troughs, flattening the dune and reducing the lee side slope (Martin & Jerolmack, 2013).

At the study site, the discharge has been stable for over 7 months, rendering it unlikely that the larger dunes are a relict from the last discharge peak that faded away at end of January. However, it has been shown that especially after floods with short falling limbs, primary dunes can be in disequilibrium with the prevailing flow conditions for long periods of time (Leary & Ganti, 2020; Myrow et al., 2018). Following a flood, during which large dunes have formed, a large mass redistribution is necessary for large dunes to adapt or disappear, whereas the sediment transport capacity is low.

Myrow et al. (2018) proposed a framework to assess whether bedforms in a system are in equilibrium or disequilibrium with the prevailing flow conditions, namely the dimensionless bedform disequilibrium number, T^*:

$$T^* = \frac{T_f}{T_t}, \tag{10}$$

where T_f is the duration of the prevailing flow and T_t is the bedform turnover timescale:

$$T_t = LH\beta / q_s, \tag{11}$$

with $\beta \approx 0.55$. For $T^* < 1$, bedforms are in disequilibrium with the flow, whereas for $T^* > 1$, bedforms have sufficient time to adapt to the changing flow conditions.

We apply this framework to investigate whether the primary dunes observed in the study area can be considered relicts of prior peak discharge, or, alternatively, are in (near-)equilibrium with the prevailing flow. We computed T^* based on the hydrograph presented in Figure 1, the primary dune properties (Figure 5) and the sediment transport rates (Figure 7). We computed T_t for all datapoints and present the distribution of the obtained values in Figure 8, as well as the hydrograph and the time it takes for T^*_{P50} and T^*_{P95} to reach a value of one (based on the 50th and 95th percentile of T_t, respectively). Figure 8 demonstrates that the primary dunes have had ample time to adapt from the peak discharge at the end of January 2018.

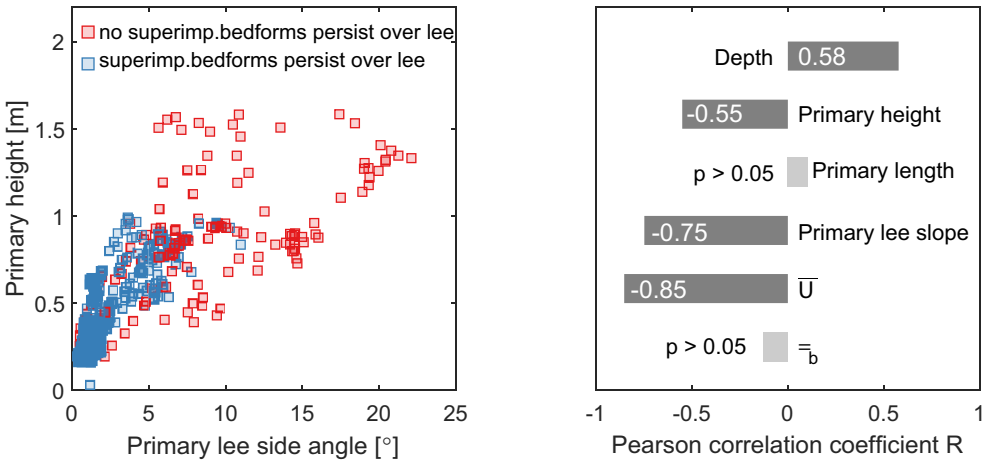

Figure 9. Left: Heights and lee side slopes of primary dunes. Right: Pearson correlation coefficients indicating the correlation between secondary bedform height on the one hand and depth, primary dune properties (height, length, lee slope), and flow properties ($\overline{u}$, τ_b) on the other hand. For the computation or the correlation between the depth and secondary bedform height, all values have been included. For the correlation with primary dune properties, transect averaged values have been used. For the computation of correlation with $\overline{u}$ and τ_b, transect-averaged values of secondary bedform height have been used, interpolated to correspond to the y-coordinate at which $\overline{u}$ and τ_b have been defined. The presented correlation coefficients are significant ($p < 0.05$), except for the correlation with primary dune length and τ_b.

Further considering that the primary dunes have high lee side angles at their central axes and the fact that the primary dunes are actively migrating over the full river width (Figures 6 and 7), the superimposition of secondary bedforms here cannot be explained as cannibalism of relict dunes.

When the superimposition of secondary bedforms is observed under steady flow, they are expected to have developed in an internal boundary layer that re-establishes on the primary dune stoss. The development of the superimposed bedforms is then similar to the development of bedforms on a flat bed (Ashley, 1990; Rubin & McCulloch, 1980; Smith & McLean, 1977). Findings by Venditti et al. (2005b) based on flume experiments support this theory. In their flume experiments, the sand sheets that are superimposed on the stoss of primary dunes are similar to those developing over a flat bed (Venditti et al., 2005a, 2005b). The near-bed flow dynamics in this case are similar between primary dunes and a flat bed. Bed elevation profiles shown in Figure 4 reveal that where superimposed bedforms are not present in the primary dune trough, they start to develop some distance downstream of the trough. This might be at a distance where the boundary layer has sufficiently re-established itself, downstream of the flow reattachment point.

The data presented herein shows that at some locations the superimposed bedforms dissipate in the lee of primary dunes, which confirms previous observations by Venditti et al. (2005b). At other locations, however, superimposed bedforms travel over the dune lee and trough. Figure 4 indicates an influence of the primary lee slope. To further study this, the primary lee slope and height (trough to crest) were determined (Figure 9, left panel). The properties are calculated for every 10th transect of the bathymetric map. It was visually determined in which areas secondary bedforms were either or not superimposed on the dune lee and trough.

Figure 9 indicates that at primary lee slopes larger than approximately 11°, no superimposed bedforms occur. This is a lower value than that found by Galeazzi et al. (2018). They studied compound dunes with and without superimposed bedforms on the lee side and found that for dunes with superimposed bedforms on the lee side the primary lee side angle is generally below 15–18°.

We suggest two mechanisms through which the primary lee side slope controls whether or not superimposed bedforms dissipate when entering the lee side slope. First, for primary lee slopes near or at the angle of repose, superimposed bedforms might simply disintegrate because of sediment avalanching. Second, the flow structure over the primary dunes might play an important role. For dunes with steeper lee side

angles, the boundary layer developed over the dune stoss side does not persist over the lee side. Short-scale flow expansion and deceleration over the dune lee leads to flow separation as well as high turbulence production (Kwoll et al., 2016; Naqshband et al., 2014b), causing the disintegration of the secondary bedforms reaching the lee. For low-angle dunes on the other hand, it has been shown that flow separation is not or intermittently present and turbulence production is significantly lower (Kwoll et al., 2016). This can allow superimposed bedforms to pass through the primary troughs.

Prior research indicates that (permanent) flow separation disappears at a lee side slope ranging from 11° to 20° (Bradley et al., 2013; Kwoll et al., 2017; Lefebvre & Winter 2016). The slope for which permanent flow separation is present, has been indicated to depend on dune height relative to the depth, where flow separates at lower slopes for dunes with a larger relative dune height (Lefebvre & Winter 2016). The angle for which flow separates might further depend on the bed grain size distribution and the prevailing flow velocity.

Figure 9a also shows datapoints for which superimposed do not persist over low lee side angles. These datapoints are primarily located in the western sections, where superimposed bedforms are absent in the proximity of steep lee side angles or not well resolved by the MBES measurements over larger areas.

4.2. Lateral Variation in Secondary Bedform Properties

The secondary bedforms vary laterally in size and shape. The bedforms are superimposed on large three-dimensional lunate dunes which are steepest over their central axes and have much more gradual lee side slopes toward their sides, which extend from both the west and east sections toward the center (Figures 3–5). The underlying river bed also varies in elevation with higher elevation at the eastern river bank compared to the western bank (Figure 1). Figures 1 and 7 further indicate strong lateral variation in the flow velocity and the bed grain size distribution.

We quantified the linear relationships between the secondary bedform height on the one hand and the local depth, primary dune properties and flow properties ($\overline{u}, \tau_b$) on the other. The Pearson correlation coefficients (R) are presented in Figure 9b. Figure 9b indicates a moderate correlation with depth and primary height. There is no significant correlation ($p > 0.05$) with the primary dune length and the bed shear stress, τ_b. Correlation is strongest with the primary lee side slope and depth averaged flow velocity. The bed grain size is not included in the analysis, because within the study area the number of samples is limited.

We first discuss the correlation with primary dune height and lee side slopes, which are inevitably linked. We hypothesize that the correlation with secondary bedform height depends on the flow structure over and downstream of primary dunes, which depends on the relative dune height and lee side angle. Downstream of steep lee side slopes, a stronger turbulent wake develops starting from the flow reattachment point (Bennett & Best, 1995; Kwoll et al., 2016; Venditti & Bennett, 2000). This turbulent wake confines the internal boundary layer on the downstream dune stoss and by that might limit the vertical space in which secondary bedforms can develop. Downstream of low lee side angles, the wake is significantly weaker (Best & Kostaschuk, 2002; Kwoll et al., 2016; Lefebvre et al., 2016). The flow over the crests of low-angle dunes shows more resemblance to flow over a flat bed (Kwoll et al., 2016). Liu et al. (2020) showed the co-evolution of developing sand waves and the near bed flow, indicating the importance of the boundary layer for the development and growth of bedforms.

Second, the secondary bedform height correlates with lateral variations in the depth-averaged flow velocity and local river bed elevation. Though the upstream 4–5 km of the river channel is relatively straight, in general, the curvature of the Waal river affects the river bed morphology, with stable point bars located in inner bends (de Ruijsscher et al., 2020). Within the study area, the eastern section is shallower, whereas the western section is deeper, but decreases in depth in the downstream direction. At the western bank, a point bar develops approximately 0.5 km downstream (de Ruijsscher et al., 2020). The river bed morphology and weak curvature upstream might explain the flow distribution, with higher flow velocities along the western bank.

Previous studies have indicated that an increase in water depth seems more favorable to the superimposition of secondary bedforms (Galeazzi et al., 2018; Reesink et al., 2018), which is different from what we observe here. The flow velocity might affect the overall flow structure over the primary dunes and through that affect the development of superimposed bedforms.

Bed samples further indicate that the bed sediments are coarser in the western section of the river compared to the eastern section (Figure 1). Wilbers (2004) has attributed this typical pattern in grain size variation to the effect of navigation. Draw down currents generated by passing ships lead to a delivery of fine sediments from eroding beaches to the main channel. This effect is more pronounced for the (south-)eastern part of the river, because the ships sailing upstream, from the port of Rotterdam to Germany, typically stay close to the southeastern river bank and carry a heavier load. The variation in grain size has previously been connected to a lateral variation in dune properties in the river Waal (Wilbers, 2004), where primary river dunes in the southeastern section are lower and shorter (Wilbers & Ten Brinke, 2003). This matches with our observations and might indirectly affect the secondary bedform size, which have been shown to negatively correlate with the primary dune height. Whether the superimposed bedform properties are also directly affected by the bed grain size is not clear.

In a final note regarding the lateral variation of bedform size, the bedforms in the central section have a large relative height compared to the primary dunes and have steep lee side angles (Figure 5). Here, the superimposed bedforms might be dominant in controlling the local flow structure. It has also been shown before that superimposed bedforms with a relatively large height compared to their host (25–30%) reduce the hosts bedform lee slope (Reesink & Bridge, 2007), creating even more favorable conditions for secondary bedform growth.

4.3. Sediment Transport Rates Associated With Secondary and Primary Bedform Migration

The transport rate associated with secondary bedform migration is of the same order of magnitude as that inferred from primary dune migration, and partly even exceeds the latter estimate (Figure 7). Though smaller, the secondary bedform migrate faster than the primary dunes. It has been shown before that small-scale bedforms tend to move faster and large-scale bedforms slower (Coleman & Melville, 1994; Guala et al., 2014, 2020). The observations presented here add field evidence to a suggestion made by Venditti et al. (2005b), who argued that, under conditions where secondary bedforms are superimposed on high-angle dunes, sediment transport rates are likely invariant to bedform scale. In addition, when comparing migration rates of smaller and larger secondary bedforms, the average bedform elevation, $\overline{\eta}$, inversely correlates to migration celerity, V_c ($R = -0.68$, $p < 0.05$).

The bed sediment transport was also estimated following Engelund and Hansen (1967) (Figure 7d). Since the ratio of the bed shear velocity to the particle fall velocity is low (Figure 7b), the bed sediments are predominantly transported as bedload, enabling comparison with the estimates based on dune tracking. The calculated transport is of the same order of magnitude as the sediment transport rates calculated based on dune tracking. The values are comparable over the full river width, except for a peak around $y = 20$ m. The peak in the calculated transport results from a peak in the bed shear stress at that location. This peak in bed shear stress does not correspond to any peak in sediment transport associated with bedform migration. Though the transport based on Engelund and Hansen (1967) is similar to that based on dune tracking and thus supports the validity of the used dune tracking method, uncertainty in the calculated transport limits a precise, quantitative comparison.

To assess what the overall impact is of multiscale bedform migration on the total sediment transport inferred from tracking of primary dunes only, the question arises to what extent the transport rate associated with secondary bedform migration contributes to primary dune migration. When superimposed bedforms travel over the stoss side and dissipate across the primary dune lee side, they are fully accounted for in bedload transport rates inferred from primary dune migration tracking. In the other extreme, when superimposed bedforms uninterruptedly travel through the primary dune troughs, transport rates inferred from primary dune tracking are an underestimation. Here, at least a subtle interaction is likely to occur. Secondary bedforms may cause the migration of a primary dune by causing net erosion of the primary stoss, which is

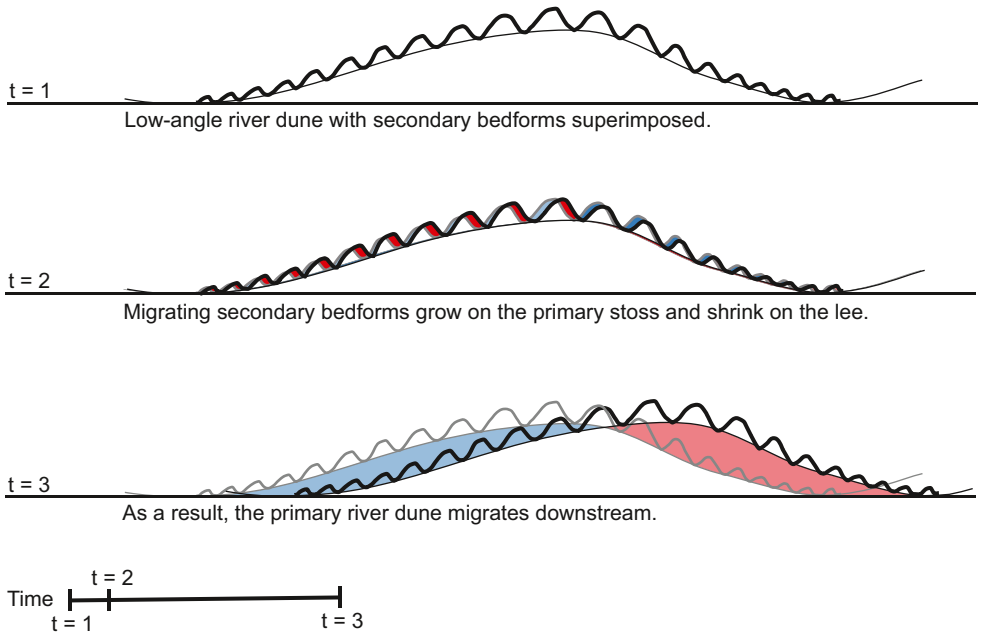

Figure 10. Schematic illustrating the hypothesis concerning the interaction and co-migration of two bedform scales.

when the secondary bedforms grow, and causing net deposit of sediment at the lee side, which is when the secondary bedforms shrink (Figure 10). The sediment transport associated with secondary bedform migration then varies depending on the position on the primary dune. To further investigate this, high-resolution MBES measurements are needed at different locations on the primary dune, such that the spatial pattern in sediment transport associated with secondary bedform migration can be studied.

Even though the interaction between bedform scales is not clear and it is unknown what the additional contribution of secondary bedforms is to the total sediment transport, the presented results demonstrate that sediment transport calculations based on tracking of primary dunes only can lead to significant underestimations. The temporal resolution of repeated bed elevation scans chosen for dune tracking confines the bedform scale for which the associated transport rate can be calculated. Before dune tracking can be applied in river sections with multiscale bedform migration, it needs to be understood how separate scales interact, and by that, to what extent transport rates associated with distinct scales overlap or add up.

5. Conclusions

The aim of this study is to investigate the morphodynamics of multiscale fluvial bedforms and the associated implications for sediment transport rates. For this purpose, bed elevation surveys with a high spatiotemporal resolution were conducted in the Dutch river Waal, and compared to MBES data acquired on a lower temporal resolution. Results indicate that both primary dunes and superimposed, secondary bedforms actively migrate over the full river width. The bedload sediment transport associated with the migration of the smaller, superimposed bedforms equals or even exceeds the bedload transport rates associated with primary bedform migration. This is because the trains of smaller bedforms migrate with a much higher celerity than primary dunes.

Previous research suggested that secondary bedforms fully dissipate on the primary lee slopes and thus contribute to migration of the primary dunes. Our results demonstrate that secondary bedforms can travel over the lee side of primary dunes. One of the controlling factors determining whether superimposed bedforms dissipate at the primary lee side or not, is the primary dune morphology, specifically the primary lee side angle, where on lee side angles below 11° secondary bedforms can persist.

Interaction of dune dynamics at multiple scales determines the quality of bedload sediment transport estimations inferred from tracking of primary dunes. It remains to be discovered what conditions enable the development of superimposed bedforms within a fluvial system, and how well-developed superimposed bedforms in turn affect flow dynamics and the overall sediment transport in a system.

Data Availability Statement

The ADCP data and gridded bathymetric data can be retrieved through https://doi.org/10.4121/13517384. The Matlab scripts for separating bathymetric data representing multiple bedform scales are archived though https://doi.org/10.5281/zenodo.4486604. The toolbox for processing ADCP data, developed by Bart Vermeulen, is available through https://sourceforge.net/projects/adcptools.

Acknowledgments
This study is part of the research program Rivers2Morrow, which is funded by the Dutch Ministry of Infrastructure and Water Management and its executive organization Rijkswaterstaat. A.J.F. Hoitink and S. Naqshband were partially funded by the Netherlands Organization for Scientific Research (NWO), within Vici project "Deltas out of shape: regime changes of sediment dynamics in tide-influenced deltas" (Grant NWO-TTW 17062). Funding for the field campaign was provided by Rijkswaterstaat Oost-Nederland, within the WaalSamen program. We thank Alice Lefebvre and two anonymous reviewers for their helpful comments and suggestions.

References

Allen, J. (1966). On bed forms and palaeocurrents. *Sedimentology*, *6*(3), 153–190. https://doi.org/10.1111/j.1365-3091.1966.tb01576.x

Allen, J. (1985). *Principles of physical sedimentology*. London: Allen & Unwin.

Allen, J., & Collinson, J. (1974). The superimposition and classification of dunes formed by unidirectional aqueous flows. *Sedimentary Geology*, *12*(3), 169–178. https://doi.org/10.1016/0037-0738(74)90008-6

Ashley, G. M. (1990). Classification of large-scale subaqueous bedforms; a new look at an old problem. *Journal of Sedimentary Research*, *60*(1), 160–172. https://doi.org/10.2110/jsr.60.160

Bagnold, R. A. (1966). *An approach to the sediment transport problem from general physics*. US Government Printing Office.

Bennett, S., & Best, J. (1995). Mean flow and turbulence structure over fixed, two-dimensional dunes: Implications for sediment transport and bedform stability. *Sedimentology*, *42*(3), 491–513. https://doi.org/10.1111/j.1365-3091.1995.tb00386.x

Best, J., & Kostaschuk, R. (2002). An experimental study of turbulent flow over a low-angle dune. *Journal of Geophysical Research*, *107*(C9), 3135. https://doi.org/10.1029/2000JC000294

Bradley, R., Venditti, J., Kostaschuk, R., Church, M., Hendershot, M., & Allison, M. A. (2013). Flow and sediment suspension events over low-angle dunes: Fraser Estuary, Canada. *Journal of Geophysical Research: Earth Surface*, *118*(3), 1693–1709. https://doi.org/10.1002/jgrf.20118

Bradley, R. W., & Venditti, J. G. (2017). Reevaluating dune scaling relations. *Earth-Science Reviews*, *165*, 356–376. https://doi.org/10.1016/j.earscirev.2016.11.004

Carling, P., Golz, E., Orr, H., & Radecki-Pawlik, A. (2000). The morphodynamics of fluvial sand dunes in the river rhine, near Mainz, Germany. i. sedimentology and morphology. *Sedimentology*, *47*(1), 227–252. https://doi.org/10.1046/j.1365-3091.2000.00291.x

Cheng, N.-S. (2009). Comparison of formulas for drag coefficient and settling velocity of spherical particles. *Powder Technology*, *189*(3), 395–398. https://doi.org/10.1016/j.powtec.2008.07.006

Cisneros, J., Best, J., Van Dijk, T., de Almeida, R. P., Amsler, M., & Boldt, J. (2020). Dunes in the worlds big rivers are characterized by low-angle lee-side slopes and a complex shape. *Nature Geoscience*, *13*(2), 156–162. https://doi.org/10.1038/s41561-019-0511-7

Claude, N., Rodrigues, S., Bustillo, V., Bréhéret, J.-G., Macaire, J.-J., & Jugé, P. (2012). Estimating bedload transport in a large sand–gravel bed river from direct sampling, dune tracking and empirical formulas. *Geomorphology*, *179*, 40–57. https://doi.org/10.1016/j.geomorph.2012.07.030

Cleveland, W. S. (1979). Robust locally weighted regression and smoothing scatterplots. *Journal of the American Statistical Association*, *74*(368), 829–836. https://doi.org/10.1080/01621459.1979.10481038

Coleman, S. E., & Melville, B. W. (1994). Bed-form development. *Journal of Hydraulic Engineering*, *120*(5), 544–560. https://doi.org/10.1061/(ASCE)0733-9429(1994)120:5(544)

Davies, T. R. (1982). Lower flow regime bedforms: Rational classification. *Journal of the Hydraulics Division*, *108*(3), 343–360. https://doi.org/10.1061/JYCEAJ.0005834

de Ruijsscher, T., Naqshband, S., & Hoitink, A. (2020). Effect of non-migrating bars on dune dynamics in a lowland river. *Earth Surface Processes and Landforms*, *45*(6), 1361–1375. https://doi.org/10.1002/esp.4807

de Ruijsscher, T., Vermeulen, B., & Hoitink, A. (2020a). Diversion of flow and sediment toward a side channel separated from a river by a longitudinal training dam. *Water Resources Research*, *56*, e2019WR026750. https://doi.org/10.1029/2019WR026750

de Ruijsscher, T., Vermeulen, B., & Hoitink, A. (2020b). *Replication data for: Diversion of flow and sediment toward a side channel separated from a river by a longitudinal training dam4tu.researchdata. Dataset*. Retrieved from https://doi.org/10.4121/uuid:a2b6bb99-b984-4d30-bbb8-bacd80f251ad

Eleftheriou, A., & Moore, D. C. (2013). Macrofauna techniques. In A. Eleftheriou (Ed.), *Methods for the study of marine benthos* (4th ed., pp. 175–251). Oxford: John Wiley & Sons, Ltd.

Engel, P., & Lau, Y. (1980). Computation of bed load using bathymetric data. *Journal of the Hydraulics Division*, *106*(3), 369–380. https://doi.org/10.1061/JYCEAJ.0005380

Engelund, F., & Hansen, E. (1967). *A monograph on sediment transport in alluvial streams*. Copenhagen: Technical University of Denmark.

Galeazzi, C. P., Almeida, R. P., Mazoca, C. E., Best, J. L., Freitas, B. T., Ianniruberto, M., et al. (2018). The significance of superimposed dunes in the Amazon River: Implications for how large rivers are identified in the rock record. *Sedimentology*, *65*(7), 2388–2403. https://doi.org/10.1111/sed.12471

GDAL/OGR Contributors. (2020). *GDAL/OGR geospatial data abstraction software library [Computer software manual]*. Retrieved from https://gdal.org

Greenslade, D. J., Chelton, D. B., & Schlax, M. G. (1997). The midlatitude resolution capability of sea level fields constructed from single and multiple satellite altimeter datasets. *Journal of Atmospheric and Oceanic Technology*, *14*(4), 849–870. https://doi.org/10.1175/1520-0426(1997)014<0849:TMRCOS>2.0.CO;2

Guala, M., Heisel, M., Singh, A., Musa, M., Buscombe, D., & Grams, P. (2020). A mixed length scale model for migrating fluvial bedforms. *Geophysical Research Letters*, *47*(15), e10.1029/2019GL086625. https://doi.org/10.1029/2019GL086625

Guala, M., Singh, A., BadHeartBull, N., & Foufoula-Georgiou, E. (2014). Spectral description of migrating bed forms and sediment transport. *Journal of Geophysical Research: Earth Surface*, *119*(2), 123–137. https://doi.org/10.1002/2013JF002759

Harbor, D. J. (1998). Dynamics of bedforms in the lower Mississippi River. *Journal of Sedimentary Research*, *68*(5), 750–762. https://doi.org/10.2110/jsr.68.750

Hendershot, M. L., Venditti, J. G., Bradley, R. W., Kostaschuk, R. A., Church, M., & Allison, M. A. (2016). Response of low-angle dunes to variable flow. *Sedimentology*, *63*(3), 743–760. https://doi.org/10.1111/sed.12236

Hoitink, A., Buschman, F., & Vermeulen, B. (2009). Continuous measurements of discharge from a horizontal acoustic doppler current profiler in a tidal river. *Water Resources Research*, *45*(11), W11406. https://doi.org/10.1029/2009WR007791

Holmes, R. R., Jr, & Garcia, M. H. (2008). Flow over bedforms in a large sand-bed river: A field investigation. *Journal of Hydraulic Research*, *46*(3), 322–333. https://doi.org/10.3826/jhr.2008.3040

Julien, P., Klaassen, G., Ten Brinke, W., & Wilbers, A. (2002). Case study: Bed resistance of rhine river during 1998 flood. *Journal of Hydraulic Engineering*, *128*(12), 1042–1050. https://doi.org/10.1061/(ASCE)0733-9429(2002)128:12(1042)

Kleinhans, M., Wilbers, A., & Ten Brinke, W. (2007). Opposite hysteresis of sand and gravel transport upstream and downstream of a bifurcation during a flood in the River Rhine, the Netherlands. *Netherlands Journal of Geosciences/Geologie en Mijnbouw*, *86*(3). https://doi.org/10.1017/S0016774600077854

Kostaschuk, R. (2000). A field study of turbulence and sediment dynamics over subaqueous dunes with flow separation. *Sedimentology*, *47*(3), 519–531. https://doi.org/10.1046/j.1365-3091.2000.00303.x

Kostaschuk, R., Shugar, D., Best, J., Parsons, D., Lane, S., Hardy, R., et al. (2009). Suspended sediment transport and deposition over a dune: Río Paraná, Argentina. *Earth Surface Processes and Landforms*, *34*(12), 1605–1611. https://doi.org/10.1002/esp.1847

Kostaschuk, R., & Villard, P. (1996). Flow and sediment transport over large subaqueous dunes: Fraser River, Canada. *Sedimentology*, *43*(5), 849–863. https://doi.org/10.1111/j.1365-3091.1996.tb01506.x

Kwoll, E., Venditti, J., Bradley, R., & Winter, C. (2016). Flow structure and resistance over subaquaeous high-and low-angle dunes. *Journal of Geophysical Research: Earth Surface*, *121*(3), 545–564. https://doi.org/10.1002/2015JF003637

Kwoll, E., Venditti, J., Bradley, R., & Winter, C. (2017). Observations of coherent flow structures over subaqueous high-and low-angle dunes. *Journal of Geophysical Research: Earth Surface*, *122*(11), 2244–2268. https://doi.org/10.1002/2017JF004356

Leary, K. C., & Ganti, V. (2020). Preserved fluvial cross strata record bedform disequilibrium dynamics. *Geophysical Research Letters*, *47*(2), e2019GL085910. https://doi.org/10.1029/2019GL085910

Lefebvre, A., Paarlberg, A. J., & Winter, C. (2016). Characterizing natural bedform morphology and its influence on flow. *Geo-Marine Letters*, *36*(5), 379–393. https://doi.org/10.1007/s00367-016-0455-5

Lefebvre, A., & Winter, C. (2016). Predicting bed form roughness: The influence of lee side angle. *Geo-Marine Letters*, *36*(2), 121–133. https://doi.org/10.1007/s00367-016-0436-8

Liu, Y., Jiang, X., Lee, C., & Hu, H. (2020). An experimental study on the spatiotemporal evolution of sand waves/ripples in turbulent boundary layer airflow. *Physics of Fluids*, *32*(6), 063304. https://doi.org/10.1063/1.5144522

Martin, R. L., & Jerolmack, D. J. (2013). Origin of hysteresis in bed form response to unsteady flows. *Water Resources Research*, *49*(3), 1314–1333. https://doi.org/10.1002/wrcr.20093

McElroy, B., & Mohrig, D. (2009). Nature of deformation of sandy bed forms. *Journal of Geophysical Research*, *114*(F3), F00A04. https://doi.org/10.1029/2008JF001220

Myrow, P. M., Jerolmack, D. J., & Perron, J. T. (2018). Bedform disequilibrium. *Journal of Sedimentary Research*, *88*(9), 1096–1113. https://doi.org/10.2110/jsr.2018.55

Naqshband, S., & Hoitink, A. (2020). Scale-dependent evanescence of river dunes during discharge extremes. *Geophysical Research Letters*, *47*(6), e2019GL085902. https://doi.org/10.1029/2019GL085902

Naqshband, S., Ribberink, J. S., & Hulscher, S. J. (2014a). Using both free surface effect and sediment transport mode parameters in defining the morphology of river dunes and their evolution to upper stage plane beds. *Journal of Hydraulic Engineering*, *140*(6), 1–6. https://doi.org/10.1061/(ASCE)HY.1943-7900.0000873

Naqshband, S., Ribberink, J. S., Hurther, D., & Hulscher, S. J. (2014b). Bed load and suspended load contributions to migrating sand dunes in equilibrium. *Journal of Geophysical Research: Earth Surface*, *119*(5), 1043–1063. https://doi.org/10.1002/2013JF003043

Nelson, J. M., McLean, S. R., & Wolfe, S. R. (1993). Mean flow and turbulence fields over two-dimensional bed forms. *Water Resources Research*, *29*(12), 3935–3953. https://doi.org/10.1029/93WR01932

Nelson, J. M., Shreve, R. L., McLean, S. R., & Drake, T. G. (1995). Role of near-bed turbulence structure in bed load transport and bed form mechanics. *Water Resources Research*, *31*(8), 2071–2086. https://doi.org/10.1029/95WR00976

Parsons, D. R., Best, J. L., Orfeo, O., Hardy, R. J., Kostaschuk, R., & Lane, S. N. (2005). Morphology and flow fields of three-dimensional dunes, Rio Paraná, Argentina: Results from simultaneous multibeam echo sounding and acoustic doppler current profiling. *Journal of Geophysical Research*, *110*(F4), F04S03. https://doi.org/10.1029/2004JF000231

Reesink, A., & Bridge, J. (2007). Influence of superimposed bedforms and flow unsteadiness on formation of cross strata in dunes and unit bars. *Sedimentary Geology*, *202*(1–2), 281–296. https://doi.org/10.1016/j.sedgeo.2009.09.014

Reesink, A., Parsons, D., Ashworth, P., Best, J., Hardy, R., Murphy, B., et al. (2018). The adaptation of dunes to changes in river flow. *Earth-Science Reviews*, *185*, 1065–1087. https://doi.org/10.1016/j.earscirev.2018.09.002

Rubin, D., & McCulloch, D. (1980). Single and superimposed bedforms: A synthesis of San Francisco Bay and flume observations. *Sedimentary Geology*, *26*(1–3), 207–231.

Schlax, M. G., & Chelton, D. B. (1992). Frequency domain diagnostics for linear smoothers. *Journal of the American Statistical Association*, *87*(420), 1070–1081.

Simons, D. B., Richardson, E. V., & Nordin, C. F. (1965). Bedload Equation for Ripples and Dunes (Vol. 462). US Government Printing Office.

Smith, J. D., & McLean, S. (1977). Spatially averaged flow over a wavy surface. *Journal of Geophysical Research*, *82*(12), 1735–1746. https://doi.org/10.1029/JC082i012p01735

Ten Brinke, W., Wilbers, A., & Wesseling, C. (1999). *Dune growth, decay and migration rates during a large-magnitude flood at a sand and mixed sand-gravel bed in the Dutch Rhine river system*. In Fluvial Sedimentology Vi (Vol. 28, pp. 15–32). Wiley Online Library.

Van der Mark, C., & Blom, A. (2007). A new and widely applicable tool for determining the geometric properties of bedforms. *Water Engineering and Management*, 1568–4652.

Van der Mark, C., Blom, A., & Hulscher, S. (2008). Quantification of variability in bedform geometry. *Journal of Geophysical Research*, *113*(F3), F03020. https://doi.org/10.1029/2007JF000940

Van Rijn, L. C. (1984). Sediment transport, part ii: Suspended load transport. *Journal of Hydraulic Engineering*, *110*(11), 1613–1641. https://doi.org/10.1061/(ASCE)0733-9429(1984)110:11(1613)

Venditti, J. G., & Bennett, S. J. (2000). Spectral analysis of turbulent flow and suspended sediment transport over fixed dunes. *Journal of Geophysical Research*, *105*(C9), 22035–22047. https://doi.org/10.1029/2000JC900094

Venditti, J. G., Church, M. A., & Bennett, S. J. (2005a). Bed form initiation from a flat sand bed. *Journal of Geophysical Research*, *110*(F1), F01009. https://doi.org/10.1029/2004JF000149

Venditti, J. G., Church, M., & Bennett, S. J. (2005b). Morphodynamics of small-scale superimposed sand waves over migrating dune bed forms. *Water Resources Research*, *41*(10), W10423. https://doi.org/10.1029/2004WR003461

Vermeulen, B., Sassi, M., & Hoitink, A. (2014). Improved flow velocity estimates from moving-boat adcp measurements. *Water Resources Research*, *50*(5), 4186–4196. https://doi.org/10.1002/2013WR015152

Warmink, J. J., Dohmen-Janssen, C. M., Lansink, J., Naqshband, S., van Duin, O. J., Paarlberg, A. J., et al. (2014). Understanding river dune splitting through flume experiments and analysis of a dune evolution model. *Earth Surface Processes and Landforms*, *39*(9), 1208–1220. https://doi.org/10.1002/esp.3529

Wilbers, A. (2004). *The development and hydraulic roughness of subaqueous dunes*. Faculty of Geosciences, Utrecht University.

Wilbers, A., & Ten Brinke, W. (2003). The response of subaqueous dunes to floods in sand and gravel bed reaches of the Dutch Rhine. *Sedimentology*, *50*(6), 1013–1034. https://doi.org/10.1046/j.1365-3091.2003.00585.x